Conformation of β-Methylmelibiose Bound to the Ricin B-Chain As Determined from Transferred Nuclear Overhauser Effects†

V. L. Bevilacqua, Yangmee Kim, and J. H. Prestegard*

Department of Chemistry, Yale University, New Haven, Connecticut 06511

Received March 10, 1992; Revised Manuscript Received July 6, 1992

ABSTRACT: Transferred nuclear Overhauser effect (TRNOE) experiments have revealed a change in the torsion angles about the α-1–6 glycosidic bond of methyl β-melibioside upon binding of the melibioside to the ricin B-chain (Rb). A full relaxation rate matrix simulation of experimental buildup curves aided in quantitative interpretation of 1D selective inversion recovery TRNOE experiments. The data are consistent with a model in which both major ($\omega \approx 170°$) and minor ($\omega \approx -60°$) conformers for methyl β-melibioside are significantly populated in solution while the Rb/methyl β-melibioside complex has little of the minor conformer populated. The results indicate that the ricin B-chain excludes binding of certain ligand conformations on the basis of unfavorable interactions between the protein surface and remote portions of the disaccharide system.

Control of such important biological processes as growth and fertilization, as well as defense against invading organisms, requires that a cell interact with its environment at the level of its external membrane surface. The interactions often involve the binding of a protein to an oligosaccharide receptor anchored to the membrane as a part of an integral glycoprotein or glycolipid. Specific examples include the actions of hormones, antibodies, and lectin-like cell adhesion molecules. Knowledge of the structural details of such protein–carbohydrate interactions is fundamental to understanding the interplay between a cell and its environment and to the logical design of pharmaceuticals that mimic the action of natural systems. Thus, much current research has been directed at understanding the nature of the protein–carbohydrate recognition process.

Emphasis, so far, has centered on the role of specific hydrogen bond-forming groups on the protein and the precise fit of these groups with hydroxyl functions on the sugar most directly involved in recognition (Vyas et al., 1991; Quiocho, 1990, 1989). Crystal structures of proteins complexed with relatively small ligands have played a prominent part in the development of this picture. Most of these crystal structures are of periplasmic binding proteins complexed with monosaccharides. Yet a much wider array of proteins participates in the recognition process, and many of these bind to larger oligosaccharides. Although remote residues of these larger oligosaccharides seem to modify specificity and alter binding constants, the structural basis for the role of these remote residues remains less clear. Carver (1989) suggests that a protein–oligosaccharide interaction will restrict the ligand conformations. In this instance, the protein binding site is not believed to change significantly upon binding. As the size of the ligand increases, it has more contact with the protein surface, resulting in more restriction on the conformation about the linkages of the ligand. On the other hand, others have proposed that the more exposed surfaces of proteins are quite mobile and may be able to adopt to specific ligand conformations (Eftink et al., 1983: Hindsgaul et al., 1985). As the size of the ligand increases, the protein surface at the binding site becomes more structured. For either case, interactions between the protein surface and the extended portions of the ligand are important and warrant more experimental investigation.

Plant lectins (which specifically bind carbohydrates) provide suitable systems for the exploration of the binding modes of various saccharides. While once thought of as a system relegated to the plant kingdom, recent research has identified a number of vertebrate lectins (Caron et al., 1990; Phillips et al., 1990; Walz et al., 1990; Osborn, 1990; Couraud et al., 1989; Drickamer, 1988). In addition, several mammalian proteins containing lectin-like domains have been implicated in the inflammatory response (Phillips et al., 1990; Walz et al., 1990; Osborn, 1990). Here we choose a particularly well characterized plant lectin (the ricin B-chain) as a model of the types of ligand–protein interactions common to all of these systems. The ricin B-chain (Rb,[1] MW 34 000) is the lectin portion of ricin, a toxic protein found in castor beans. Rb binds to galactose-terminated oligosaccharides on the cell surface and mediates transport of the toxic A-chain (MW 31 000) into the cell where it disrupts protein synthesis (Houston & Dooley, 1982).

Conflicting evidence exists as to the interaction of extended portions of ligand molecules with the B-chain. The crystal structure of Rb complexed with lactose implies that specific hydrogen bonds between certain galactose hydroxyls and Rb residues dominate the recognition process (Rutenber & Robertus, 1991). The glucose ring appears to be free in solution and does not interact with the protein. In addition, a crystal structure of a biantennary oligosaccharide with Rb implicates the same galactose contacts with the protein, while the sugar residues beyond galactose do not appear to interact with the protein (Rutenber & Robertus, 1991). Thus, the crystal structure evidence supports a theme which emphasizes primary interaction with the terminal sugar. On the other hand, the K_a's for naturally occurring cell surface oligosaccharides are 1000 times greater than those for simple saccharides (Baenziger & Fiete, 1979). Also, Rb shows some

† This work was supported by the National Institutes of Health, Grant GM19035.

* Author to whom correspondence should be addressed.

[1] Abbreviations: Rb, ricin B-chain; SIR, selective inversion recovery; FID, free induction decay; NOE, nuclear Overhauser effect; TRNOE, transferred nuclear Overhauser effect; τ_m, mixing time; rmsd, root mean square deviation.

0006-2960/92/0431-9339$03.00/0

specificity for β- over α-galactose-terminated ligands (Yamasaki et al., 1985), suggesting some importance for the position of sugar rings beyond the terminal galactose. A study of various methyl β-lactoside derivatives, in fact, suggested an important interaction between the protein and position 3 of the glucose ring (Rivera-Sagredo et al., 1991). This work correlated binding kinetics with free ligand solution conformations determined by molecular mechanics calculations and NMR data.

Our NMR work on methyl β-lactoside employed the transferred nuclear Overhauser effect (TRNOE) in an effort to detect conformational changes in the sugar induced by binding to the protein. Such a change would require that remote interactions provide a driving force. The work did show some tendency of protein binding to restrict conformational freedom about the glycosidic bond (Bevilacqua et al., 1990). However, induced changes were rather small, leaving in question the nature of any remote interactions. Possibly, only small changes can take place since the β-1–4 linkage of lactose contains just two torsional angles, for which a fairly limited range of conformers is available.

We present here transferred nuclear Overhauser effect experiments on the Rb/methyl β-melibioside system. Methyl β-melibioside (methyl 6-*O*-α-D-galactopyranosyl-β-D-glucopyranoside) contains an α-1–6 linkage and consequently possesses three variable torsion angles about the glycosidic linkage. Accordingly, melibiose is expected to be more flexible than lactose in solution and offers the possibility of selection from a broader range of populated conformers. The structure of any specific conformation selected will be analyzed in terms of the interaction of the protein with the ligand residues beyond the terminal galactose.

The transferred nuclear Overhauser effect has been extensively investigated as a means of determining the structure of a ligand when bound to a protein (Campbell & Sykes, 1991; Bevilacqua et al., 1990; Clore et al., 1986; Andersen et al., 1985; Clore & Gronenborn, 1982). The TRNOE is based on cross relaxation among protons on the ligand, just as NOEs employed in protein structure determination are based on cross relaxation among protein protons. Experimentally, the magnetization associated with one spin is perturbed (in our case by selectively inverting its resonance). A fixed period of time (the mixing time, τ_m) is allowed for transfer of magnetization by cross relaxation. Magnetization associated with each spin is then observed by analyzing the free induction decay following a 90° pulse. In ideal cases, the magnetization transfer between two spins is proportional to $1/r^6$, where r is the distance between the spins. These distances can be converted to a structure using any number of structure determination protocols.

The TRNOE experiment, however, differs from the simple NOE experiment in that chemical exchange transmits information about the bound state to the free state, allowing observation of bound-state NOEs through the better resolved and more easily detected free ligand resonances. In many cases experiments can be conducted with a high ratio of ligand to protein, facilitating work with sparingly soluble proteins. Furthermore, the TRNOE makes possible the study of ligand binding to large proteins, even when excessive line broadening would preclude direct observation of the protein resonances. The reason that indirect observation via a TRNOE works is that the relaxation processes that establish an NOE in the bound state are far more efficient than those that establish an NOE in the free state. NOEs grow in proportion to a cross-relaxation rate that depends on the difference in efficiencies between a zero-quantum and a two-quantum process. For moderately large molecules the zero-quantum process dominates, and the growth of an NOE is proportional to its rotational correlation time, τ_c. Correlation times are roughly proportional to effective molecular weight, so a ligand binding to a protein ten times its size would have a bound-state NOE established ten times faster than a free-state NOE. As long as exchange between bound and free states is fast compared to spin relaxation ($>10^2\ s^{-1}$), a population-weighted average of bound and free NOEs is seen. Clearly, even with a 5-fold excess of ligand over protein, the bound-state NOE will dominate. In practice, ligands are often sufficiently small that the zero-quantum process does not dominate. In these cases, establishment of the free-state NOE is even less efficient. It also occurs with an opposite sign. The change of sign between bound-state and free-state NOEs provides an additional qualitative indication that the bound-state NOE is dominating a TRNOE measurement.

Obviously a number of complications can arise when the ideal conditions described above are not met. For a moderately large protein, as opposed to a very large one, the domination of an averaged NOE is not nearly so complete. NOEs cannot then be simply interpreted as being proportional to the inverse sixth power of the separation between protons in the bound state. Contributions from the free state must be explicitly included.

For very large proteins on the other hand, cross relaxation may become so efficient that not only pairwise NOE transfers but also successive NOE transfers to other spins (spin diffusion) might require consideration. The necessity of considering these additional transfers can be minimized by keeping mixing times short. This is analogous to the approach usually used in direct NOE studies of macromolecules. In some cases keeping mixing times short in TRNOE experiments is even easier because effective residence time on the protein is scaled by the protein-to-ligand ratio and longer times can be used. However, choosing short mixing times is not always practical, particularly when ligand-exchange rates become slow ($\sim 100\ s^{-1}$). In these cases, exchange between free and bound pools cannot scale down the effective mixing time, and restrictions on length of mixing times become more severe.

Our previous study of the methyl β-galactoside/Rb system addressed some of the complications associated with nonideal behavior (Bevilacqua et al., 1990). We found that a simulation of 1D selective inversion recovery curves that explicitly considered each ligand spin, as well as a ligand-exchange rate and the presence of free ligand, was practical. Thus, the analysis of TRNOE 1D selective inversion recovery experiments to be presented here will be aided by the previously developed programs for complete relaxation matrix simulation.

EXPERIMENTAL PROCEDURES

Materials. Ricin B-chain in phosphate-buffered saline solution and methyl β-galactoside were purchased from Sigma Chemical Co., St. Louis, MO. SDS gels of the initial protein sample showed a single major spot running with approximate molecular weight 34 000 and a minor (<10%) spot running with a slightly lower molecular weight. Comparison of ^1H NMR spectra of a D_2O solution of the protein to that of a well-characterized pure sample (Bushuev & Tonevitsky, 1989) also showed no significant differences. The material was therefore used without further purification. Analysis of Rb samples by affinity chromatography on Sepharose 4B (Sigma) after extensive use and storage indicated that >85% of the Rb retained its ability to bind galactose during the course of our studies.

Methyl β-melibioside was synthesized from melibiose (Sigma Chemical Co.) using the method of Smith and Van Cleve (1952). Briefly, melibiose (5.0 g) was converted to the octaacetate ($NaOAc/Ac_2O$, 100 °C, 99% yield). The product was then converted to the bromoheptaacetate (crude yield = 92%) using saturated HBr in $HOAc/Ac_2O$ (1:1). Crude bromoheptaacetate (3.16 g) was dissolved in MeOH and stirred overnight with Ag_2CO_3 in the dark. The reaction mixture was filtered through Celite, rotovapped, and placed under vacuum until dry. The methyl heptaacetate was purified from 1.0 g of the crude product by flash chromatography on a silica gel column [ethyl acetate/hexane (1:1), 35% yield]. The acetates were removed by stirring the solution overnight in the presence of NaOMe in MeOH followed by neutralization with Dowex 50 (H^+ form), filtration, and removal of methanol with a rotovap. The final product was dissolved in H_2O, filtered through Chelex, and lyophilized. The yield of methyl β-melibioside, judged from ^1H NMR spectra to be >90% pure, from the methyl heptaacetate was 83%.

Sample Preparation. Sugar NMR samples were prepared by repeated lyophilization and D_2O exchange as in the past (Bevilacqua et al., 1990). Rb/sugar samples were prepared using Centricon-10 microconcentrators (Amicon, Danvers, MA), to effect D_2O exchange. For each sample, a total of 6.00 mL of D_2O buffer (99.9% D) was used for exchange: 3 × 2.00 mL of buffer containing 2.50 mM methyl β-galactoside for the Rb/galactoside sample and 2 × 2.00 mL plus 2 × 1.00 mL of buffer containing 3.00 mM methyl β-melibioside for the Rb/melibioside sample. The final concentrated samples were brought to 0.36 mL (Rb/melibioside) and to 0.44 mL (Rb/galactoside) with deuterated buffer (99.96% D) containing sugar at the desired concentration. The Rb concentration of the Rb/galactoside sample was 0.24 mM as determined by UV absorbance of a volumetric dilution of the sample ($E^{1\%}_{280nm,1cm}$ = 14.9; Olsnes et al., 1975). The Rb concentration of the Rb/melibioside sample was determined to be 0.23 mM by comparison of Rb and sugar peak ratios of its NMR spectrum to ratios in spectra for the Rb/galactoside sample and a previous Rb/lactoside sample in which the Rb concentration was determined from UV measurements.

Buffers were at pH 6.5 (uncorrected for isotope effects) and contained 10 mM phosphate, 0.15 M NaCl, and 0.02% NaN_3. All buffered samples were purged 10 min with N_2 and used immediately or stored desiccated under N_2 at 4 °C. The methyl β-melibioside COSY sample (used simply for assignment purposes) was not buffered or purged.

NMR Procedures. ^1H NMR data were collected at 30 °C with quadrature detection on a home-built 490-MHz spectrometer and transferred to a VAXSTATION 3500 or to a VAXSTATION 3200 for processing. To aid in free methyl β-melibioside spectral assignments and scalar coupling constant determinations, a double-quantum-filtered COSY spectrum of methyl β-melibioside (61 mM) was acquired using time-proportional phase incrementation (TPPI; Marion & Wüthrich, 1983). The spectrum was collected using a sweep width of 1131 Hz with 2048 t_2 points and 512 t_1 points of 16 scans each. The set was processed using a sine-bell weighting function and zero filling to 2048 points in both dimensions. In addition, high-resolution 1D spectra of the COSY sample (0.37 Hz/point) and a buffered sample (0.24 Hz/point) were collected and used in coupling constant determinations.

To provide an accurate determination of NOE buildup curves 1D selective inversion recovery (SIR) difference experiments were carried out as outlined earlier (Bevilacqua et al., 1990). Briefly, a single soft pulse of 0.015-s duration was used to selectively invert the 4.93 ppm H1′ (galactose ring) resonance. Mixing times (τ_m) from 0.200 to 3.000 s for the free melibioside and 0.100 to 1.200 s for melibioside in the presence of Rb were allowed for inversion recovery and NOE transfer. Then, a single hard pulse sampled the spectrum. A very short mixing time FID was also collected to determine the amount of inversion of H1′. In order to accumulate adequate signal-to-noise ratios, different numbers of scans were accumulated at different mixing times in accordance with the intensity of the NOE expected for that mixing time. In each case an equivalent reference spectrum was produced by placing the soft pulse 2813 Hz downfield of 4.93 ppm, where no protein or sugar resonances are expected. Pairs of spectra at each time point were subtracted to produce difference spectra showing NOEs. For each mixing time, several well-resolved, single-proton ligand peaks in the reference spectrum were integrated with standard processing software, and the average integral was set equal to one proton. Well-resolved, single-proton peaks in the difference spectra were also integrated with standard software. However, curve fitting using commands available in FTNMR (Hare Research Inc., Woodenville, WA) was used to obtain the areas of overlapping peaks. Comparison of integrals obtained by curve fitting well-resolved peaks and peaks artificially broadened to produce significant overlap suggests little degradation in precision from that obtained by direct integration of well-resolved peaks, about 1.5%. The difference NOEs were recorded as a fraction (relative NOE) or percentage (% NOE) of the area of one proton and should reflect this precision.

A two-dimensional phase-sensitive NOESY spectrum was acquired for free methyl β-melibioside (3 mM) using the method of States et al. (1982) and a mixing time of 800 ms. The sweep width was 1000 Hz with a size of 2048 t_2 points. The number of FIDs was 128 with 64 scans in each FID and a delay of 5 s between scans. For processing, t_1 was zero filled to 2048 points and a cosine-bell weighting function was used in both dimensions. A two-dimensional TRNOESY for the Rb/methyl β-melibioside sample was also acquired in the phase-sensitive mode by the States method. However, because of poor resolution and sensitivity, only the anomeric rows proved useful.

Simulations. Time–course simulations were carried out using the program previously described (Bevilacuqa et al., 1990). This program uses the geometric position of every free and bound ligand proton to calculate dipole–dipole interactions among spins and then employs a complete relaxation method to calculate the magnetization intensities during the times following selective inversion of one or more of the spins. In order to obtain structures for use in calculating dipole–dipole interactions, energy minimizations were carried out on free methyl β-melibioside in a vacuum using AMBER[2] with a force field modified for carbohydrates (Scarsdale et al., 1988). The initial methyl β-melibioside structure was created from the crystal structure of α-melibioside (Gress et al., 1978). The glucose anomeric proton and hydroxyl group of α-melibioside were replaced by a β-methoxy group and an α-proton, respectively, using bond distances, bond angles, and torsion angles from a previously minimized structure containing a methyl-β-glucose ring. The resulting methyl β-melibioside structure was minimized (structure 0), and starting structures for all subsequent single-state minimizations

[2] AMBER (3.1 and 3.0; U. C. Singh, P. K. Weiner, D. A. Case, J. Caldwell, and P. A. Kollman, 1986) is a program obtained through a licensing agreement with the Regents of the University of California at San Francisco.

were obtained by systematically varying the glycosidic torsion angles of this initial, minimized methyl β-melibioside.

Because of conformational averaging which can occur in solution, single rigid conformers often fail to be suitable models for spin relaxation data in solution. To address this possibility, two- and three-state combinations of the single-state structures were also generated. These were found using a version of AMBER modified to include an equilibrium between groups of conformers (Kim & Prestegard, 1990). Constraints derived from initial slope estimations of NOE effects and from measurements of vicinal couplings about the H5–H6 exocyclic bond of glucose were included by adding a penalty proportional to the deviation between an experimental observable and the weighted average of observables calculated for each member of the equilibrating combination. The scalar coupling equations used to evaluate dihedral constraints about C5–C6 were derived from Haasnoot's-modified Karplus equations (Haasnoot et al., 1980) using parameter set *D*. These are summarized as

$$J_{5,6a} = 13.22(\cos^2\theta_1) - 0.99(\cos\theta_1) + 2.61 - 0.984\{\cos^2(\theta_1 + 7.96)\} - 3.198\{\cos^2(-\theta_1 + 25.87)\} \quad (1)$$

$$J_{5,6b} = 13.22(\cos^2\theta_2) - 0.99(\cos\theta_2) + 2.61 - 0.984\{\cos^2(\theta_2 + 7.96)\} - 6.396\{\cos^2(-\theta_2 + 25.87)\} \quad (2)$$

θ_1 and θ_2 represent the torsion angles between H5 and H6a and between H5 and H6b, respectively. Initially, equilibrium constants were selected to produce the best fit of experimental data using a given set of structures from single-state minimizations carried out without constraints. Next, a two-state minimization routine with stepwise modulation of constraint weighting functions was carried out to further adjust the conformation of the initial structures. This routine is similar to that previously used for multiple-state treatments of protein systems (Kim & Prestegard, 1990).

Briefly, three minimization cycles were used: the first with heavy weights of experimental constraints and only bond and bond angle terms for molecular energies, the second with heavy weights of experimental constraints and all terms for molecular energies, and the third with light weights of experimental constraints and all terms for molecular energies. Weights in this last case corresponded to a penalty of approximately 10 kcal for the complete absence of a 3-Å NOE, or a violation of more than 2 Hz in a coupling constant calculated from a trial combination of structures. Minimizations were carried out using a combination of steepest descent and conjugate gradient minimizers. A constant dielectric of 50 was assumed with short-range (1–4) electrostatic and van der Waals terms scaled by factors of 4 and 2, respectively. Convergence usually occurred due to the norm of the gradient falling below 10^{-3} kcal/(mol Å). Typical times for convergence on a VAXSTATION 3500 were 45 min.

RESULTS AND DISCUSSION

Figure 1 shows a possible structure (structure 0) for methyl β-melibioside and depicts the three variable torsion angles involved in the α-1–6 linkage between the glucose and galactose residues. The α-1–6 linkage invites special interest because the ricin B-chain appears to have a lower affinity for α- versus β-galactose-terminated oligosaccharides (Yamasaki et al., 1985). A comparison of free versus bound methyl β-melibioside may provide some insight as to the reason for this selectivity. The choice of values for the glycosidic bond torsion angles ϕ, ψ, and ω in the linkage are almost totally responsible

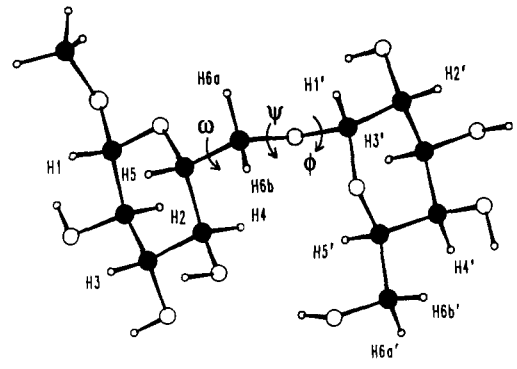

FIGURE 1: Structure 0, initial AMBER-minimized methyl β-melibioside structure (see Experimental Procedures). $\phi = -39°$, $\psi = -165°$, $\omega = 170°$.

for the overall shape of the disaccharide since they define the relative position of the fairly inflexible sugar rings. In describing the torsion angles, we use the convention that ϕ = H1′–C1′–O6–C6, ψ = C1′–O6–C6–C5, and ω – O6–C6–C5–H5. The sign of the angle is defined as being positive when the remote bond, looking along the bond from the second to the third atom, is rotated in a clockwise direction. The glucose protons are labeled H1–H6, while the galactose protons are labeled H1′–H6′.

Free Ligand Conformation. In principle, analysis of ^{1}H–^{1}H scalar coupling and NOE data should lead to definition of the solution structure of free methyl β-melibioside. Vicinal coupling data between protons at the C5 and C6 positions of the glucose ring should be particularly useful in determination of ω. NOEs between the galactose H1′ and glucose protons such as the H6a, H6b, and H5 should provide help in evaluating ϕ and ψ. Although we do not expect artifacts arising from spin diffusion for the free disaccharide, analysis problems connected with populations of multiple conformational states may arise. Before we proceed with the analysis, however, chemical shift assignments must be made.

Assignment of the spectrum proceeded on the basis of high-resolution COSY and 1D spectra (see Figure 2). The downfield chemical shifts and scalar couplings of the peaks at 4.93 and 4.35 ppm readily identified them as α-H1′ and β-H1, respectively. Straightforward assignment of the remaining ring protons resulted from following the COSY cross peaks. Integration of the 1D spectrum affirmed that the multiplet centered at 3.92 ppm represents three protons (assigned to H5′, H4′, and H6b). Likewise, the doublet centered at 3.69 ppm represents two protons (the H6′ protons). Since H6a′ and H6b′ (galactose ring) are undistinguishable in chemical shift (3.69 ppm) in nonbuffered samples, only an average *J* value can be determined (6.2 Hz). However, in 1D spectra recorded with buffered samples, the H6′ shifts diverge and the apparent $J_{H5',6'}$ couplings differ by 1 Hz. This divergence is consistent with values measured for stereospecifically deuterated analogues (Nishida et al., 1984) if the smaller coupling is assigned to H6b′ and the larger to H6a′. Rather than extract couplings from highly second-order systems, we shall assume that Nishida's values are relevant to our system. In the case of the glucose ring, comparison of the H6 chemical shifts and $J_{H5,6}$ couplings to those for stereospecifically deuterated β-methyl α-1–6 diglucosides (Ohrui et al., 1985) allowed assignment of the upfield H6 peak to H6a (δ = 3.73 ppm, $J_{5,6a}$ = 2.1 Hz) and the downfield H6 peak to H6b (δ = 3.92 ppm, $J_{5,6b}$ = 4.7 Hz). Table I lists the chemical shifts and coupling constants for free methyl β-melibioside.

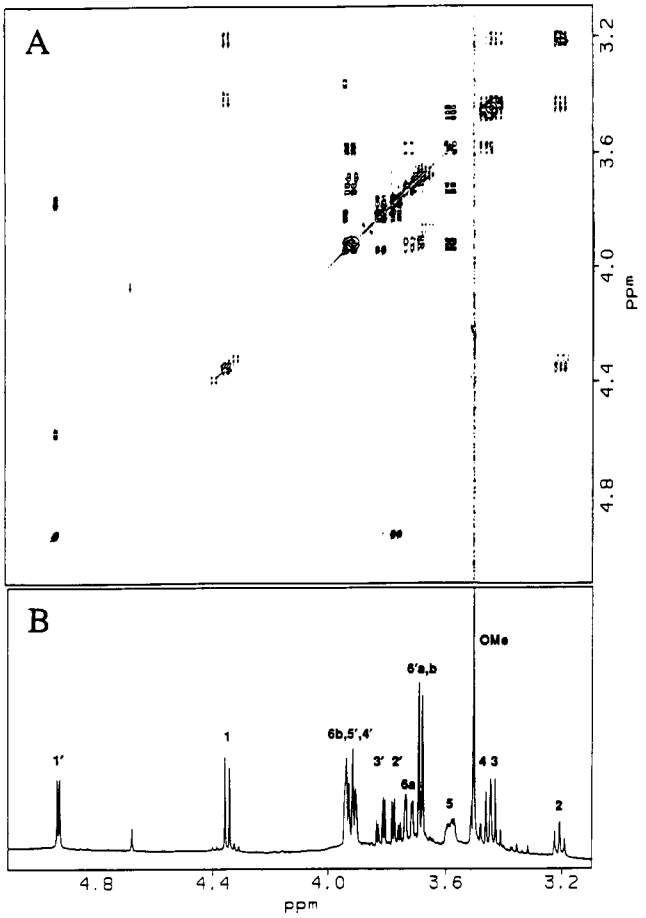

FIGURE 2: (A) Methyl β-melibioside COSY spectrum. The spectrum shown was processed with zero filling to 1K points in the t_1 dimension and a sine bell in both dimensions. (B) Methyl β-melibioside (61 mM in D_2O) ^1H NMR spectrum. The FID was collected with a sweep width of 1131 Hz and processed in a manner similar to that of the t_2 dimension of the COSY spectrum.

Table I: Chemical Shifts and Scalar Couplings for Methyl β-Melibioside

proton	δ[a] (ppm)	proton pair	J (Hz) 2D (±0.5 Hz)	J (Hz) 1D (±0.4 Hz)
H1′	4.93	H1′–H2′	3.8	3.7
H2′	3.77	H2′–H3′	10.4	10.3
H3′	3.82	H3′–H4′	3.3	3.2
H4′	3.94	H4′–H5′		
H5′	3.92	H5′–H6′	6.2	6.3
H6′ (a,b)	3.69	H6′–H6′		
H1	4.35	H1–H2	8.0	8.1
H2	3.21	H2–H3	8.6	~8.8
H3	3.43	H3–H4	8.8	~8.8
H4	3.46	H4–H5	9.7	9.8
H5	3.58	H5–H6a	2.3	1.8
H6a	3.73	H5–H6b	4.6	4.7
H6b	3.92	H6a–H6b	−11.1	−11.4
OMe	3.50			

[a] Chemical shift relative to the HDO peak at 4.67 ppm.

Pyranose sugar rings of glucose and galactose are generally regarded as predominantly occupying the chair forms. $J_{H1,2}$ and $J_{H1',2'}$ are consistent with α- and β-anomeric configurations for the glucose and galactose rings, respectively. The $J_{H2,3}$, $J_{H3,4}$, $J_{H2',3'}$, and $J_{H3',4'}$ values are consistent with both rings residing in $^4C_1$ chair conformations. The coupling constants for the 6′ protons (galactose), taken from Nishida et al. (1984), imply a dynamic equilibrium about the galactose methylene group with an approximate population ratio of 27:36:37. It is

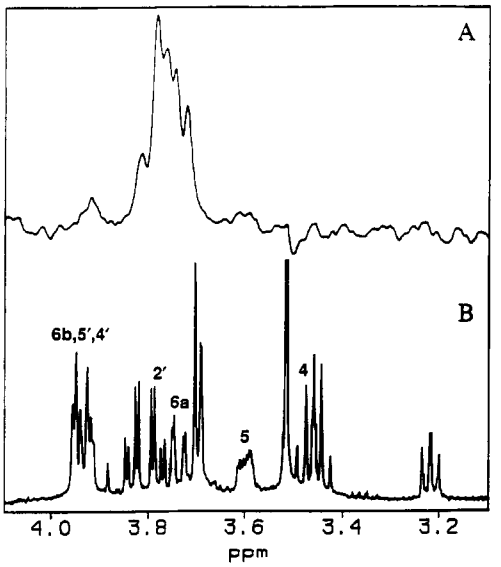

FIGURE 3: (A) ^1H SIR NOE spectrum of methyl β-melibioside (3 mM in buffer; τ_m = 0.800 s; sweep width = 2000 Hz; size = 8K). H1′ (4.94 ppm) was selectively inverted in one spectrum. An equivalent pulse at 10.68 ppm was applied in a second spectrum. FIDs resulting from 536 scans were transformed using a line broadening of 5.0 Hz and subtracted. (B) ^1H NMR methyl β-melibioside spectrum (sweep width = 2000 Hz; size = 8K).

noteworthy, however, that both major conformers have one H6′ proximate to H5 and one H6′ farther from H5 and that the distances to the far and near protons are identical for the two major conformers. In terms of the spin system geometry used in theoretical calculations of cross relaxation, the two conformers are, therefore, identical. We propose to use the major conformer to represent the two most populated states of this group and neglect the presence of the minor conformer. In any event, the galactose 6′ methylene group is remote from the glycosidic linkage protons which play a direct role in determining the conformation of melibioside. The H5–H6 coupling constants of the glucose ring indicate a minimum of two conformers differing in angle about the C5–C6 bond in solution, with major and minor rotamers having ω values of approximately 180° and −60°, respectively, and a population ratio of 70:30 (Ohrui et al., 1985). More information is necessary to describe the φ and ψ torsion angles.

In order to obtain additional information about the glycosidic linkage, a 1D NOE SIR time–course experiment was carried out. H1′ presents a good choice for inversion because it offers several possible transfers to other protons throughout the glycosidic region and because the isolated H1′ peak furnishes an excellent target for inversion selectivity. Also, an expected H1′–H2′ NOE for the chair form of galactose could be used for calibration in distance calculations. Figure 3A shows a difference spectrum with a mixing time of 0.800 s. The anticipated H1′–H2′ transfer occurs, as well as several important NOEs across the glycosidic bond: a strong one to H6a and small ones to H6b and H5. Figure 4A shows the experimental NOE buildup curves for H2′, H6a, H6b, and H5. Although small, the H6b and H5 NOEs appear at all time points, increasing confidence in these observations. These small NOEs might initially be mistaken for spin diffusion from H6a to H6b and H5. However, diffusion for free methyl β-melibioside would be opposite in sign from primary transfers whereas all transfers here are positive. A 2D NOESY also recorded (not shown) shows essentially the same H1′ NOEs and relative intensities as for the 1D experiment.

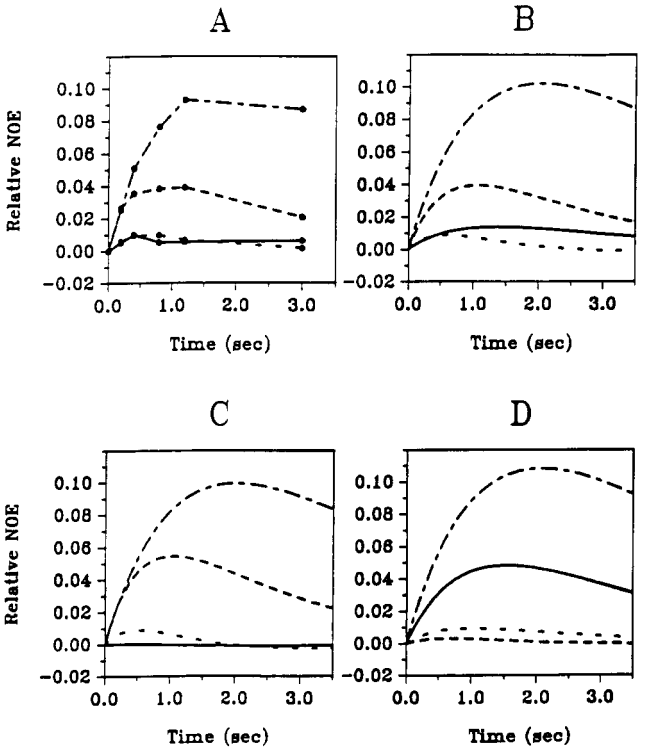

FIGURE 4: NOE buildup curves for free methyl β-melibioside: H2′ (- - -), H6a (– –), H6b (- - -), and H5 (—). Relative NOE is the intensity in the difference spectra as a fraction of the intensity of one proton in the reference spectra. (A) Experimental results (●). The experimental values for H2′ were multiplied by 1.04 to take strong coupling effects between H2′ and H3′ into account, as determined by a calculation to determine the magnitude of these effects. (B) K′O simulation results (K′:O = 70:30). (C) K′ simulation results. (D) O simulation results.

A ϕ of –60° and a ψ of 180° would satisfy the strong H1′–H6a and weaker H1′–H6b NOEs. However, this ϕ/ψ pair would place H5 much too far from H1′ to result in an NOE of observable intensity for either choice of ω angle. On the other hand, a ϕ of –60°, a ψ of 120°, and an ω of –60° would be compatible with the H1′–H6a and H1′–H5 NOEs. But, this set of angles would not satisfy the H1′–H6b NOE. Obviously, one conformer cannot result in the observed trans glycosidic NOEs. Thus, in addition to variation in ω, ϕ and ψ must vary among conformers.

To establish a pool of energetically allowed conformers, we undertook a series of unconstrained minimizations starting from structures with systematic variations in ϕ, ψ, and ω. The molecular modeling package AMBER[2] was used to generate these conformers from 54 starting structures in which ϕ, ψ, and ω were altered from structure 0 (Figure 1) by rotating ϕ and ω in 120° increments and ψ in 60° increments. All possible combinations of $\phi = \pm60°$ or 180°, $\psi = 0°$, ±60°, ±120°, or 180°, and $\omega = \pm60°$ or 180° were, thus, included. In addition, six more structures resulting from unsampled combinations of $\phi = 0°$ or 180°, $\psi = 0°$ or 180°, and $\omega = 0°$ or 180° were included. Many of the starting structures converge to common structures during minimization with AMBER. In these cases we shall group structures under one name and refer to them as a "set". The resulting minimized structures fall into 25 sets with energies ranging from 5.0 to 12.1 kcal/mol. Because $J_{5,6a}$ and $J_{5,6b}$ indicate that structures with an ω of +60° will be populated ≤1% of the time (Ohrui et al., 1985), we will consider further only those structures with ω values ≠ 60°. Seventeen sets of structures then remain. Of these sets, nine display a continuous range of energies between 5.0 and 7.5 kcal/mol having gaps no greater than 0.5 kcal/mol. A single set has an energy of 8.7 kcal/mol, and the remaining sets have energies greater than 10.5 kcal/mol. One would expect that combinations of the nine lowest energy structures (5.0–7.5 kcal/mol) would dominate in solution.

Table II: Distances Calculated from Experimental NOEs for Methyl β-Melibioside

proton pair	free source[a]	distance (Å) free	distance (Å) bound
H1′–H2′	2D/1D	2.4	2.4
H1′–H6a	1D	2.5	2.5
H1′–H6b	1D	3.2	2.6 (2.8)[b]
H1′–H5	1D	3.2	3.7
H1′–H4			3.6
H1–H5		2.5	
H1–H3	2D	2.9	
H5–H6a	2D	2.8	

[a] 2D indicates distance determined from NOESY spectrum integrals. 1D indicates distance determined from 1D SIR difference spectra integrals. The H1′–H2′ distance was set to 2.41 Å. 1D distances are the average of results for two mixing times: 0.200 and 0.400 s for free and 0.100 and 0.200 s for bound. [b] This distance is calculated using 0.70 × NOE at 4.92 ppm (i.e., corrected for H5′ and H4′ contributions).

In order to further reduce the number of structures to be considered, a qualitative interpretation of NOE data was undertaken. NOEs were measured in the 1D difference spectra for the 0.200- and 0.400-s mixing times, assumed to fall in the short mixing time limit. Data from these spectra, as well as data from several rows in the 2D set, were interpreted using a simple $1/r^6$ distance relationship. Table II lists some calculated distances from 1D and 2D experiments using the H1′–H2′ distance of 2.41 Å as a calibration. In cases where multiple determinations were made, distances were averaged before inclusion in the table. The H1′–H6b distance is observed to be 3.2 Å. If only a single conformer existed, this would exclude a great many of the structures because they have shorter or longer distances. However, if the observed H1′–H6b NOE is the result of an averaging of NOEs for one conformer with a closer distance and another conformer with a longer distance, many more possibilities exist. We expect a minor conformer to be about 30% populated (Ohrui et al., 1985). However, a more conservative contribution of only 20% from a minor state would allow any structure with an H1′–H6b distance greater than 2.5 Å to participate in an equilibrium. Thus, we will consider only those structures with an H1′–H6b distance >2.5 Å. At the extreme, a combination of 20% of one conformer with a 2.5-Å H1′–H6b interproton distance and 80% of another conformer with an interproton distance longer than 4.5 Å would approximately reproduce the NOE observed, but 20% of any conformer with a distance shorter than 2.5 Å would give too large of an NOE, regardless of the nature of the second conformer. After the elimination, five sets of structures remain. Three sets have an ω of ~170°: J, K, and X. Two sets of structures have an ω of ~–60°: A and O. Table III tabulates the ϕ, ψ, ω, and energies for each set.

We now consider a number of "models" which can be constructed by considering the possibility of averaging among specific sets of structures. Six possible models exist consisting of pairs of structures containing one ω of ~60° structure and one ω of ~170° structure. This combination assures that we satisfy qualitative H1–H6 NOE data as well as H5′–H6′ coupling data, both of which require conformational averaging. The models are JA, KA, XA, JO, KO, and XO. We expect that one or more of the models will fit the experimental scalar coupling and NOE data better than any one structure alone.

Table III: Initial and Final Torsion Angles from AMBER Minimizations

initial		final		final (deg)[a]		
set	model	set	model	ϕ	ψ	ω
A		A		3	76	−65
A	JA	A	J'A	7	73	−63
A	KA	A	K'A	8	74	−63
A	XA	A	K'A	8	75	−61
O		O		−65	41	−65
O	JO	O	J'O	−70	34	−62
O	KO	O	K'O	−70	34	−62
O	XO	O''	XO''	−31	−35	−46
J		J		36	127	172
J	JA	J'	J'A	56	120	165
J	JO	J'	J'O	51	121	166
K		K		−39	−165	170
K	KA	K'	K'A	−62	−177	167
K	KO	K'	K'O	−57	176	166
X		X		−2	78	179
X	XA	K'	K'A	−54	−170	171
	XO	X	XO''	7	82	169

[a] Torsion angles pertain only to the structure designated in the third column (final, set). Where no model is listed, the angles are for the initial structure (A, O, J, K, or X).

Table IV: Initial and Final Data from AMBER Minimizations

		initial rmsd		final rmsd		
model	ratio	J (Hz)	$1/r^6$ (1/Å^6) × 10^3	J (Hz)	$1/r^6$ (1/Å^6) × 10^3	energy[a] (kcal/mol)
A	1			4.544	2.226	6.7
O	1			4.570	2.469	7.3
J	1			2.086	2.041	6.2
K	1			1.820	1.585	6.3
X	1			2.628	2.082	5.9
JA	70:30	0.380	1.942	0.016	0.431	8.2
JO	70:30	0.380	1.424	0.020	0.411	7.9
KA	70:30	0.219	1.426	0.033	0.429	8.4
KO	70:30	0.223	1.384	0.041	0.409	8.4
XA	65:35	0.721	1.991	0.088	0.437	8.3
XO	65:35	0.722	1.472	0.060	0.423	8.1

[a] Energies of single states are reported for minimizations without distance constraints. All two-state minimizations were carried out under distance and J-coupling constraints. Energies of two-state models are weighted averages of the individual conformers.

Calculated rmsd values for $J_{H5,6}$ and $1/r^6$ appear in Table IV. The $1/r^6$ rmsd was calculated by comparing experimental distances from Table II with the weighted average of $1/r^6$ in the two conformers. Scalar couplings were calculated for the AMBER structures on the basis of eqs 1 and 2, and the rmsds were again calculated by comparing the weighted average for the two structures to experimental data. Calculations were carried out for a range of ratios from 60:40 to 90:10 (major: minor). Those values shown represent the ratios which gave the best compromise between both J and $1/r^6$ fits. In each two-state model, the J fit is at least a factor of 3 better for the pair than for either structure alone. The $1/r^6$ fit is improved or equal for the two-state model relative to either structure alone. Three-state possibilities were also considered by looking at rmsd calculations (data not shown), but neither J nor NOE fits were improved over the two-state models.

The above combinations would constitute a reasonable description of molecular properties if we were sure a simple two-state model is adequate, and if we were entirely confident in the energy representation of the molecular mechanics force field. Neither is true. However, the representation can be improved by allowing NMR data to influence the conformations as long as molecular energies do not exceed our confidence limits. This can be done using a two-state energy minimization under which both conformers are allowed to adjust in the presence of experimental constraints. A version of AMBER, modified to carry out two-state minimizations using scalar coupling and NOE distance constraints, was employed for this purpose (Kim & Prestegard, 1990). Each of the six pairs of structures was minimized using distance constraints from Table II and $J_{H5,6}$ constraints. Because no H1'–H4, H2'–H6b, or H2'–H5 NOEs were observed, distances between these pairs of protons were constrained at 4.5 Å. The form of the constraint function allows large deviations to longer distances but only small deviations to shorter distances.

We will look at the results in terms of energy, J, $1/r^6$ (Table IV), and torsion angles (Table III). The average energies in each case increased by about 2 kcal/mol, which is consistent with an assumed inaccuracy of about 1 kcal/mol per residue and consistent with the range of energies in the limited set of one-state structures (±1.2 kcal/mol). The differences in average energies among pairs are small and provide little reason for choosing one pair over another. The rmsd values were calculated as above. In each case, the scalar coupling fit improved by a factor of at least 5.4, and the $1/r^6$ fit improved by a factor of at least 3.3. Again, improvements were very similar for each set.

We denote final structures which are similar to one or another of the starting sets by the one-letter designation of that set. If deviations in ϕ or ψ are between 5° and 10° a prime (') has been added to the name. When the final structure is truly unique (a ϕ or ψ change >10°), the designation of the original set has been used, but a double prime ('') has been added. With two exceptions, the final structures are similar to their starting structures. Of the exceptions, one truly unique final structure, O'', has deviated noticeably from O in the XO pair minimization. The other exception arises for minimization of the XA pair, for which the initial structure X minimized to a final structure that is similar to K. Consequently, only five two-state models remain: J'A, K'A, J'O, K'O, XO''.

If the two-state models emulate the solution equilibrium well, two-state NOE buildup curve simulations should fit the experimental buildup curves. Accordingly, two-state simulations of buildup curves were carried out using a procedure similar to that previously described (Bevilacqua et al., 1990). The major difference is that relaxation at any time point was assumed to be the population-weighted average of relaxation that occurs in each structure. This treatment assumes that the motion associated with exchange between conformers does not contribute directly to relaxation. This assumption will be true any time the lifetimes of state are significantly longer than the correlation time for molecular tumbling ($\approx 10^{-10}$ s).

The simulation was begun by fitting the H1' relaxation curve by varying τ_{cf}, where τ_{cf} is the rotational correlation time of the free molecule. Next, the H2' buildup was fit by including some external relaxation (ρ^*_f), if necessary, and varying τ_{cf} to keep the H1' fit constant. τ_{cf} ranged from 5.5 × 10^{-11} to 6.2 × 10^{-11} s, and ρ^*_f ranged from 0% to 51% of the H1' relaxation for the simulations. The total % NOE rmsd values, which are weighted over the entire recovery curve for each proton to which an NOE was observed, appear in Table V. The fits using pairs of structures after two-state minimizations were better by a factor of 2 than those using pairs of structures before two-state minimizations (data not shown). Furthermore, all simulations using the final minimized two-state structures were within experimental error of

Table V: Percent NOE rmsd Values for Melibiose Simulations[a]

	rmsd			
		bound		
model	free	both	major	minor
J'A	0.34	1.3	0.91	3.2
K'A	0.34	1.3	1.1	3.3
J'O	0.41	1.4	0.77	4.2
K'O	0.39	1.4	0.64	4.2
XO''	0.35	1.3	0.94	3.0

[a] Experimental free rmsd = 0.70; bound rmsd = 0.83. These experimental values were calculated using the experimental error for each point.

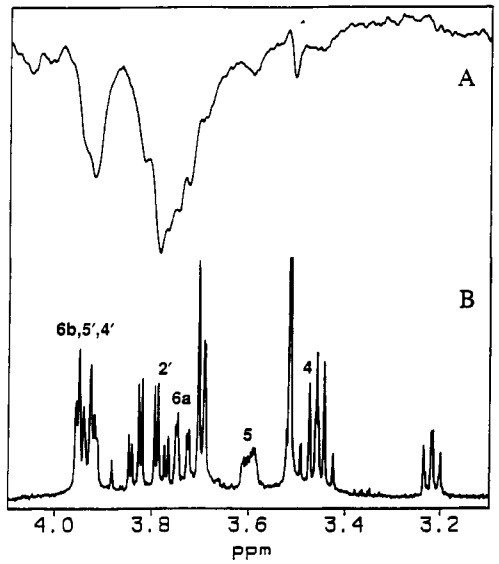

FIGURE 5: (A) TRNOE difference spectrum of methyl β-melibioside in the presence of the ricin B-chain (sugar:protein = 13:1, irradiation on H1' at 4.94 ppm; τ_m = 0.200 s; sweep width = 6024 Hz; size = 16K). FIDs resulting from 1600 scans were transformed using a line broadening of 3.0 Hz and then subtracted. (B) ^{1}H NMR spectrum of free methyl β-melibioside (sweep width = 2000 Hz; size = 8K) given for reference purposes.

the experimental data. The simulation using the K'O pair is shown in Figure 4B. Simulations with K' alone and O alone are shown in panels C and D of Figure 4 for comparison. As in the case of fits to J and $1/r^6$ derived from initial slope data described above, fits of the complete time course were very similar for each pair of structures. Therefore, the free state can be modeled well with any one of the five two-state models: J'A, K'A, J'O, K'O, or XO''. With our existing data, it is not possible to distinguish among the various models.

Bound Ligand Conformation. Figure 5A shows a 1D TRNOE difference spectrum (with H1' inverted) for methyl β-melibioside in the presence of the ricin B-chain. The sign change in NOEs compared to the free ligand NOEs establishes that the bound state dominates the NOEs of melibioside in the presence of Rb. The NOE pattern resembles that for free melibioside with strong NOEs observed at H2' and H6a and a weak NOE at H5. However, some obvious differences occur. The size of the H6b region transfer is much larger than for free melibioside. Furthermore, a new, though faint, NOE occurs at H4. Like the small H5 and H6b NOEs observed for free melibioside, the small H5 and H4 TRNOEs show up at all mixing times in a time–course experiment. These differences could imply major structural changes in melibioside upon binding to Rb.

Significant contributions from intraprotein transfers upon simultaneous inversion of protein peaks underlying the H1' peak cannot be ruled out without additional experiments. Such intraprotein transfers have been observed previously for the methyl β-lactoside/Rb system (Bevilacqua et al., 1990) and can result in enhancements which appear to be ligand NOEs. In order to check for such effects, a 1D difference control was carried out using a methyl β-galactoside/Rb sample with a similar ratio of ligand:Rb as for the melibioside experiments. The anomeric peak of methyl β-galactoside resides at a distinctly different position than the H1' of methyl β-melibioside. The inversion pulse was, therefore, set at 4.93 ppm, corresponding to H1' of methyl β-melibioside. Placing the pulse in this way should allow observation of protein–protein transfers occurring when Rb peaks at 4.93 ppm are simultaneously inverted along the H1' in the melibioside experiments. No specific intraprotein transfers were observed for the control in the sugar region. Furthermore, a 2D TRNOE spectrum of a methyl β-lactoside/Rb sample showed no specific intraprotein transfers from 4.93 ppm to positions in the sugar region. These controls rule out intraprotein transfers as the cause of intensity variations between the free and bound melibioside difference spectra.

Given the rather extensive search for allowed melibiose conformations employed in analysis of the free methyl β-melibioside data, it seems logical to look among the structures represented free in solution for an explanation of the observed changes between the free NOEs and TRNOEs. First, the free melibioside major and minor conformations may bind to Rb equally well, and all changes may be the result of extensive spin diffusion in the bound state. This would be the situation if there were no interaction of the protein with the glucose ring. Second, only one of the conformers (major or minor) may bind to Rb while the other does not. Finally, a conformation other than any of those which dominate for the free ligand may exist in the bound complex. In order to explore the binding possibilities and also to understand contributions from spin diffusion, quantitative analysis was carried out using simulation of the buildup curves.

The TRNOE simulation program operates under assumptions similar to those described for multiple conformation simulations in solution. The major differences are that motional correlation times for the bound state are quite different (larger) and ligand binding parameters, rather than a simple population ratio, are a more logical input. The program was, in fact, written to take a ligand binding constant, protein concentration, and ligand:protein ratio as input. The program assumes one binding site per protein molecule but can be used for multiple binding site cases with some reinterpretation of input.

Ricin in fact has two binding sites. Although early experimentation suggested differences of an order of magnitude in binding constants for the two sites (Zentz et al., 1978), the experiments were carried out on Rb from a different species. More recent studies indicate that the binding affinities for the two sites are very similar (Wales et al., 1991; Houston & Dooley, 1982). Thus, for our binding studies, we used a K_a of 1.8×10^3 M^{-1} (Yamasaki et al., 1985) and entered the ligand:binding site ratio rather than the ligand:protein ratio to compensate for the presence of two binding sites. Under conditions of site saturation, this compensation works reasonably well. In our previous publication, no attempt was made to compensate for the presence of two binding sites. The major effect is that the bound-state relaxation, in other words, τ_{cb}, was overestimated by approximately a factor of 2. Here, with compensation, τ_{cb} was set to 2.2×10^{-8} s (one-half the previous best-fit value). This value has a precision of

approximately $\pm 0.5 \times 10^{-8}$ s based on fits to recovery curves holding all other parameters fixed. It is also close to the value expected for a spherical protein of MW 34 000 (1.5×10^{-8} s). Correlation times (τ_{cf}) and external relaxation parameters (ρ^*_f) pertaining to the fraction of free melibiose, as opposed to melibiose bound to the protein, were set at the values determined above. Other parameters, including the external relaxation parameter (used primarily to account for the effect of protein protons) and the off rate (k_{-1}), were varied to optimize fit to the data.

For each free melibioside two-state model, three bound melibioside possibilities were considered. First, the best fit to TRNOE data was determined with the major and minor structures bound at the same population ratio as used for free melibioside. Next, the best fit with only the major conformer bound was determined. Third, the best fit with only the minor conformer bound was determined. The experimental buildup curves were simulated by first varying k_{-1} to get the best fit to the H1′ relaxation curve. Next, bound external relaxation (ρ^*_b) was added to fit H2′ with variation of k_{-1} to keep the H1′ fit constant. The value of ρ^*_b ranged from 1% to 19% of the relaxation rate of H1′, and k_{-1} ranged from 39 to 68 s^{-1}. The error in k_{-1} for a given simulation is estimated to be ± 26 s^{-1}, where the limits are set at $\pm 1/2$ of the difference in the highest and lowest k_{-1} values needed to increase the rmsd between experimental and calculated NOEs by 50% in the best fitting simulation (see below). Thus, the k_{-1} values for all simulations fall within the error of the average value.

Figure 6 shows the experimental data along with simulated TRNOE buildup curves for K′O for the three bound melibioside models considered. Figure 6D, which simulates the binding of only the minor conformer to the protein, shows the greatest deviation from experimental data (Figure 6A). The H6a and H5 curves in the simulated data are actually inverted relative to the experimental data, with H5 predicted to have a much larger NOE than that observed. Comparison of panel A with panel B in Figure 6, in which conformers are bound in the same proportions as in solution, shows better agreement. However, H6a is still too small while H5 is still too large in the simulation compared to experimental buildup curves. Figure 6C shows good agreement with experiment.

Other pairwise models in which only the major conformer is bound showed trends similar to that seen for the K′O pair. Cases in which only the major structure binds to Rb consistently show improvement in fit over the other bound melibioside models. Table V lists the % NOE rmsd values for all the simulations. These were calculated by taking the root of the mean of the squares of the differences between all experimental points in Figure 6A and their corresponding calculated values. The % NOE rmsd values for all situations where only the major structure binds are at least three times lower than those for situations where only the minor structure binds. All these structures have ω of $\approx 170°$ as opposed to $-60°$. The two TRNOE simulations with the lowest % NOE rmsd are that for the J′O pair with only J′ bound and that for the K′O pair with only K′ bound. These two models in which only the major structure binds to Rb have rmsd values 2 times lower than the rmsd values for their corresponding simulations in which the major and minor conformers bind to Rb at the same ratios as for free melibioside. It is interesting to note that K′ has glycosidic torsion angles similar to those of the α-melibioside crystal structure (see Table III) and to a global minimum found by Tvoraska for two contiguous 1–6-linked α-D-glucose residues (Tvaroska et al., 1978). J′ resembles a minimum-energy structure calculated by Tvoraska for 1–6-linked α-D-glucans. Furthermore, the J′O pair is the lowest energy pair of all the two-state possibilities considered.

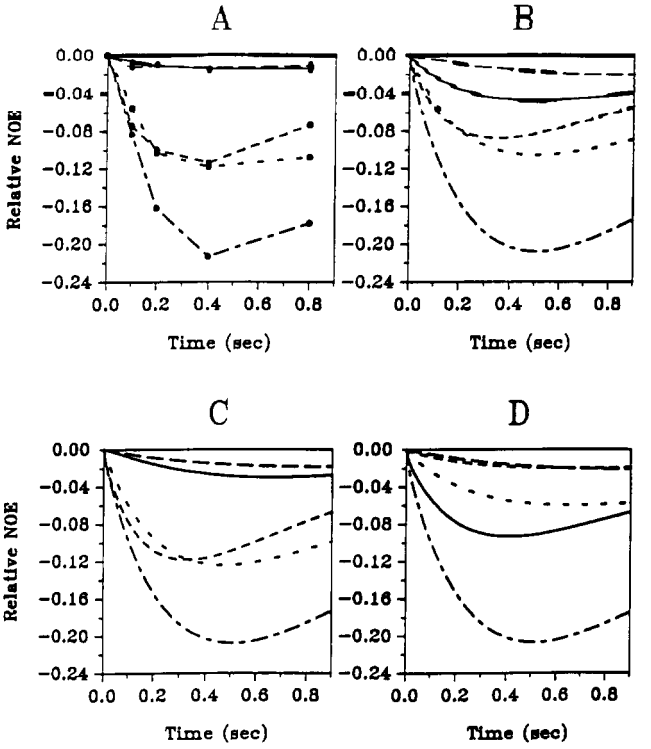

FIGURE 6: Experimental and simulated NOE buildup curves for methyl β-melibioside in the presence of Rb:H2′ (- - -), H6a (– –), H6b (- - -), H5 (—), and H4 (···). Relative NOE is the intensity in difference spectra as a fraction of the intensity of one proton in the reference spectra. All simulations have K′:O = 70:30 for free melibioside. (A) Experimental results (●). The experimental values for H2′ were multiplied by 1.04 to take strong coupling effects between H2′ and H3′ into account, as determined by a calculation to determine the magnitude of these effects. (B) Simulation results for both K′ and O bound (K′:O = 70:30). (C) Simulation results for K′ alone bound. (D) Simulation results for O alone bound.

One disturbing aspect of the apparent excellent fit of structures J′ and K′ is that neither has a short H1′–H6b distance. Yet one qualitative difference between the free and bound NOEs is the enhanced intensity at 3.92 ppm attributed to an H1′–H6b NOE. Simulation does in fact show that a good deal of this intensity comes from spin diffusion from H1′ through H6a to H6b. In addition, transfers to the poorly resolved H5′ and H4′ protons seem to contribute. Inspection of the galactose ring would cause one to expect very limited direct transfer or spin diffusion from H1′ through H2′ to H3′, H5′, and H4′. Nonetheless, simulations carried out with the H5′ and H4′ contributions separated from that of H6b revealed that an additional 30% of the intensity at 3.92 may easily result from diffusion through the galactose ring to H5′ and H4′. Therefore, a much smaller change in H1′–H6b distance most likely occurs than would be suspected from initial observation of NOE intensities.

Docking the various structures in the Rb binding sites may allow a hypothesis as to the reason for the apparent screening of conformations by Rb. The various structures were docked in the binding sites of Rb by superimposing the galactose ring atom coordinates of methyl β-melibioside with those of the lactoside galactose ring atoms present in the crystal structure (Rutenber & Robertus, 1991). Figure 7 compares K′ (the allowed conformer, Figure 7A) and O (the disallowed conformer, Figure 7B) of the K′O pair in the N-terminal binding site of Rb. The glucose ring of structure K′ extends

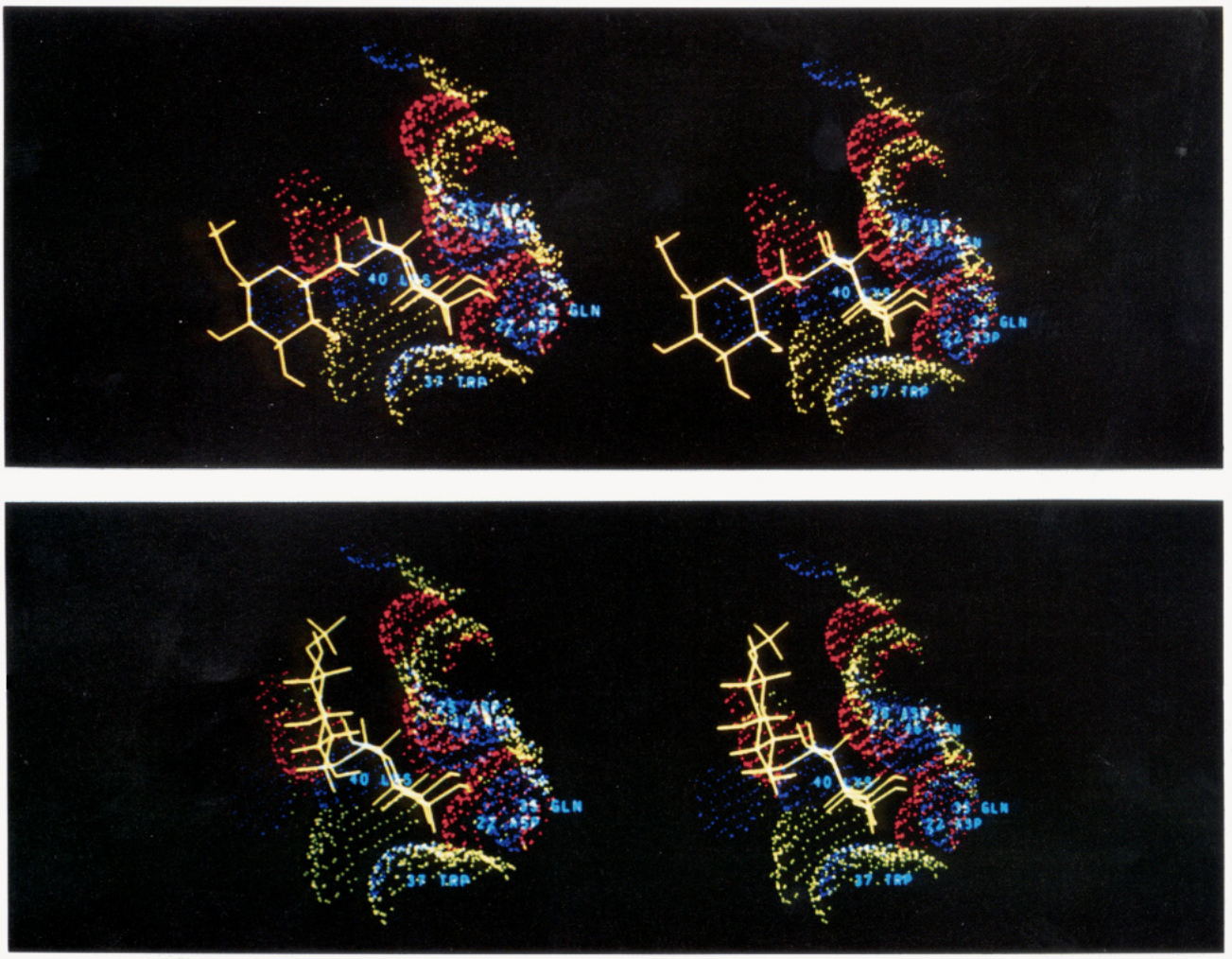

FIGURE 7: Methyl β-melibioside structures K′ (A, top) and O (B, bottom) in the N-terminal binding site of Rb.

away from the binding site into solution, remaining relatively free of interactions with protein residues. In contrast, the glucose ring of structure O sits closer to the protein surface, allowing the hydrophobic portion of the glucose ring to come within 3.0 Å of the δ-oxygen of aspartic acid 25. This placement could preclude solvation of the oxygen by solvent molecules.

Similar comparisons can be carried out for the members of the J′O, JA, K′A, and XO″ pairs. Although its glucose ring extends away from the binding site, structure J′ fits less well in the binding site than structure K′. However, a rotation of only 12° about an axis through the galactose C4 and perpendicular to the ring keeps the important H3, H4, and H6 hydrogen bonds nearly intact and brings the methyl group into a hydrophobic interaction with the aromatic ring of tryptophan 37. Thus, a very suitable structure can easily be generated. Structure X extends into solution similarly to structure K′. Structure O″ of the XO″ pair sits into the binding site similarly to O, and a similar explanation for its exclusion can be used. Structure A, however, like structures K′ and X, extends into solution. Thus, no apparent reason as to why Rb might preclude structure A is readily observable. Of course, we do not know that the J′A pair is represented in solution, only that these are consistent with the solution NMR data.

We must remember that Rb has two binding sites. They are structurally very similar, with the major difference being replacement of tryptophan in the N-terminal site (Figure 7A) with tyrosine in the C-terminal site. Visual examination shows that the placement of hydrophobic and hydrophilic surfaces in the C-terminal binding site resembles that of the N-terminal binding site. Thus, structures X, A, O, and O″ fit similarly into both binding sites. However, because the galactose ring is slightly further embedded into the C-terminal binding site, the glucose rings of structures K′ and J′ come into bad steric contact with tyrosine 248 in the exactly superimposed cases. Again, slight reorientations about C4 allow favorable placement in this binding site. In fact, the bad steric contacts translate into what could be favorable hydrophobic contacts. The same argument concerning exclusion of the O and O″ structures holds for this binding site as for the N-terminal site.

CONCLUSIONS

In summary, the solution NMR data for free methyl β-melibioside are consistent with the averaging of two conformations, a major conformer with an ω of about 170° and a minor conformer with an ω of about −60°. Significant changes in the NOEs occur upon binding to the ricin B-chain. The changes are consistent with models in which only the major conformation of the two possible free ligand conformations binds to Rb. We cannot exclude the possibility that an entirely different conformation actually exists in the methyl β-melibioside/Rb complex. However, in light of the fact that data can be fit well with single conformations believed to be represented in solution, it seems reasonable to suggest that a conformer with ω of ≈170° is bound.

Binding of such a conformer over other conformers can also be rationalized on the basis of an interaction between a

remote, nonbinding residue and the surface of the protein outside the normal binding pocket. The origin of selectivity in carbohydrate recognition is frequently attributed to selection of certain ligand conformations which are stabilized by favorable interactions, such as hydrogen bonds, with the protein. Here, no particularly important ligand–protein interactions seem evident for the glucose ring of methyl β-melibioside. Rather, an exclusion of those conformations which would require unfavorable steric or hydrophilic–hydrophobic contacts seems to occur. These exclusion interactions may in fact play an important role in recognition phenomena. External surfaces of proteins may be flexible to a degree, but even the placement of hydrophobic versus hydrophilic areas may be sufficient to contribute to greater, or lesser, levels of interaction with remote residues in potential ligands.

ACKNOWLEDGMENT

We thank Jon D. Robertus for providing the X-ray coordinates for the ricin B-chain/lactose complex and Paul-James Jones for writing the NMR integration routines.

REFERENCES

Andersen, N. H., Nguyen, K. T., & Eaton, H. L. (1985) *J. Magn. Reson. 63*, 365.
Baensiger, J. U., & Fiete, D. (1979) *J. Biol. Chem. 254*, 9795.
Bevilacqua, V. L., Thomson, D. S., & Prestegard, J. H. (1990) *Biochemistry 29*, 5529.
Bushuev, V., & Tonevitsky, A. (1989) *J. Biomol. Struct. Dyn. 6*, 1061–1070.
Campbell, A. P., & Sykes, B. D. (1991) *J. Magn. Reson. 93*, 77.
Caron, M., Bladier, D., & Joubert, R. (1990) *Int. J. Biochem. 22*, 1379.
Carver, J. P., Michnick, S. W., Imberty, A., & Cumming, D. A. (1989) *Ciba Found. Symp. 145*, 6.
Clore, G. M., & Gronenborn, A. M. (1982) *J. Magn. Reson. 48*, 402.
Clore, G. M., Gronenborn, A. M., Carlson, G., & Meyer, E. F. (1986) *J. Mol. Biol. 190*, 259.
Couraud, P.-O., Casentini-Borocz, D., Bringman, T. S., Griffith, J., McGrogan, M., & Nedwin, G. E. (1989) *J. Biol. Chem. 264*, 1310.
Drickamer, K. (1988) *J. Biol. Chem. 263*, 9557.
Eftink, M. R., Anusiem, A. C., & Biltonen, R. L. (1983) *Biochemistry 22*, 3384.
Gress, M. E., Jeffrey, G. A., & Rohrer, D. C. (1978) *Acta Crystallogr., Sect. B 34*, 508.
Haasnoot, C. A. G., de Leeuw, F. A. A. M., & Altona, C. (1980) *Tetrahedron 36*, 2783.
Hindsgaul, O., Khare, D. P., Bach, M., & Lemieux, R. U. (1985) *Can. J. Chem. 63*, 2653.
Houston, L. L., & Dooley, T. P. (1982) *J. Biol. Chem. 257*, 4147.
Kim, Y., & Prestegard, J. H. (1990) *Proteins 8*, 377.
Marion, D., & Wüthrich, K. (1983) *Biochem. Biophys. Res. Commun. 113*, 967.
Nishida, Y., Ohrui, H., & Meguro, H. (1984) *Tetrahedron Lett. 25*, 1575.
Ohrui, H., Nishida, Y., Watanabe, M., Hori, H., & Meguro, H. (1985) *Tetrahedron Lett. 26*, 3251.
Osborn, L. (1990) *Cell 62*, 3.
Phillips, M. L., Nudelman, E., Gaeta, F. C. A., Perez, M., Singhal, A. K., Hakomori, S.-I., & Paulson, J. C. (1990) *Science 250*, 1130.
Quiocho, F. A. (1989) *Pure Appl. Chem. 61*, 1293.
Quiocho, F. A. (1990) *Philos. Trans. R. Soc. London, B 326*, 341.
Rivera-Sagredo, A., Solis, D., Diaz-Mauriño, T., Jimenez-Barbero, J., & Martin-Loma, M. (1991) *Eur. J. Biochem. 197*, 217.
Rutenber, E., & Robertus, J. D. (1991) *Proteins: Struct., Funct., Genet. 10*, 260.
Scarsdale, J. N., Ram, P., & Prestegard, J. H. (1988) *J. Comput. Chem. 9*, 133.
Smith, F., & Van Cleve, J. W. (1952) *J. Am. Chem. Soc. 74*, 1912.
States, D. J., Haberkorn, R. A., & Ruben, D. J. (1982) *J. Magn. Reson. 48*, 286.
Tvaroska, I., Pérez, S., & Marchessault, R. H. (1978) *Carbohydr. Res. 61*, 97.
Vyas, N. K., Vyas, M. N., & Quiocho, F. A. (1991) *J. Biol. Chem. 266*, 5226.
Wales, R., Richardson, P. T., Roberts, L. M., Woodland, H. R., & Lord, J. M. (1991) *J. Biol. Chem. 266*, 19172.
Walz, G., Aruffo, A., Kolanus, W., Bevilacqua, M., & Seed, B. (1990) *Science 250*, 1132.
Yamasaki, N., Hatakeyama, T., & Fuantsu, G. (1985) *J. Biochem. 98*, 1555.
Zentz, C., Frénoy, J.-P., & Bourrillon, R. (1978) *Biochim. Biophys. Acta 536*, 18.

Registry No. Methyl β-melibioside, 107911-44-4.